Influence of Electrolyte Concentration on the Photocatalytic Property of Electrochemical Anodization of SnO_2 Nanostructures

Ali Jabbar Mojar[1] and Emad H. Hussein[2]

[1,2] Department of Physics, College of Science, Mustansiriyah University, Baghdad, Iraq Corresponding authors: (ali.jabar924@gmail.com,[1] emad.h@uomustansiriyah.edu.iq [2])

A B S T R A C T

In this research, new morphological SnO_2 nanostructures (Ns) prepared using a simple electrochemical anodization is described. The electrochemical process was carried out on Sn foils at a constant potential of 5 V for 10 min. To study the surface morphology effect on the photoactivity, the electrolyte concentration was chosen as the key factor using 1 mM and 5 mM. X-ray diffraction (XRD) disclosed tetragonal crystalline of SnO_2. Also, the surface morphologies imaged by a field-emission scanning electron microscope (FE-SEM) showed nanorocks and nanoparticles instead of traditional porous. Furthermore, fluorescence measurements revealed that the energy gap of SnO_2 was 3.76 eV. The photocatalytic efficiency for the discoloration of methylene blue (MB) dye was found to be 94 % after 140 min of solar irradiation. The results confirmed the connection of photoactivity with the electrolyte concentration and suggest the ability to fabricate high photocatalyst nanostructures preparation using this technique.

Keywords: *Electrochemical Anodization; SnO_2; Methylene Blue Degradation.*

1. Introduction

Properties of nanostructured materials have become crucial to the future science and technology. Among these materials, SnO_2 with a large band gap of 3.6 eV has been a strategic material due to its potential applications. It is a very stable material of high carrier density, which supports a wide range of applications like photocatalysts and gas sensors [1 – 3]. Several techniques of preparing SnO_2 Ns have been developed, including template-assisted method, electrospinning, solution-based synthesis thermal evaporation, and electrochemical anodization [4 – 7]. The electrochemical anodization has attracted interest

due to its simplicity and low cost. However, the published works reported that anodization of Sn foil may result in nanoporous [8 – 11]. Also, degradation of organic pollutants such as MB dye was already experienced by SnO_2 Ns depending on synthesis methods [12 – 14].

2. Materials and Methods

Sn foils of purity 99.9% were cut to disks of 3 cm in diameter. Then, they were cleaned by acetone in ultrasonic bath for 15 min and washed with distilled water. The experiments were achieved using two-electrode Teflon cell. The electrodes were the Sn foil sample as the anode and graphite rod as the cathode. The sample was mounted vertically in the cell body via a screw-like copper disk with a 4 cm separation from the cathode, as shown in Fig. 1. The electrolyte was a solution mixture of oxalic acid diluted by ethylene glycol. Two samples were prepared under anodization voltage of 5V and time of 10 min at 25 °C, whereas the concentration was adjusted to 1 mm for sample S1 and 5 mm for sample S2. After anodization, the samples were washed by distilled water for several times and dried thermally at 70 °C.
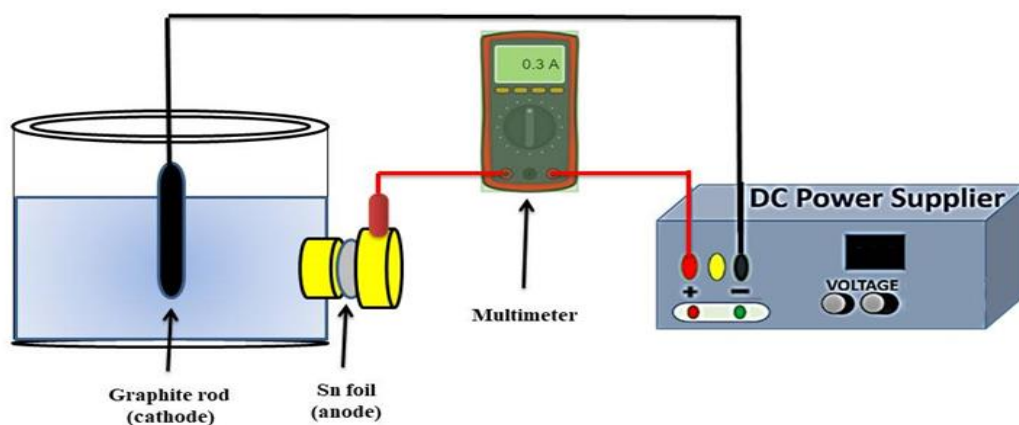
Fig. 1: Schematic illustration for the setup of the anodization experiment.

3. Characterization

The structural properties of the sample were tested by Philips X'Pert diffractometer, and their morphologies were imaged by MIRA3 TESCAN FE-SEM. Also, RF-5301 PC Shimadzu fluorophotometer was used to estimate the optical bandgap energies of the nanostructures by exciting with 280 nm light.

4. Photoactivity Tests

The SnO_2 samples with areas of 1 cm $\times$ 0.5 cm were immersed in a container of 7 ml of methylene blue dye in 1 L DW. The UV-Vis measurements were calculated using UV-Vis (LI- 2800) spectrophotometer within wavelengths from 200 nm to 900 nm. Dark measurements were done without light subjection to ensure adsorption of the dye molecules on the samples. The degradation efficiency (*Eff.*) of MB was calculated by equation (1) [15]:

$$Eff.(\%) = \frac{C_o - C_t}{C_o} \times 100 \qquad (1)$$

where C_o is the initial concentration of MB, C_t is the concentration of the irradiated dye for a certain time measured at a wavelength of 665 nm.

5. Results and Discussion
5.1 XRD measurements

The XRD patterns of the sample S1, which was fabricated in 1 mm electrolyte is shown in Fig. 2A. All the diffraction peaks, which are located at 33.22°, 58.87°, 69.66°, and 77.02° and related to the planes (101), (002), (311), and (321), respectively, are indexed as a tetragonal phase of SnO_2 according to the JCPDS card number (41-1445). Also, the peak positions of the fabricated NS are in agreement with already reported work [16]. On the other hand, a tetragonal phase of SnO is applied to the diffraction planes (101), (200), (003), and (004) according to the card (JCPDS 06-0395). The results also agree with the reported results of Iqbal *et al.* [17]. The crystallite size (D) was calculated by Debye-Scherrer equation (2) below [18].

$$D = \frac{k\,\lambda}{\beta\,cos\theta} \qquad (2)$$

where the X-ray wavelength, the Bragg diffraction angle, and the full-width at half-maximum (FWHM) are denoted by λ, θ, and β, respectively. Thus, for sample S1, the average crystallite size was found to be 12.03 nm.

The XRD pattern of sample S2, which was fabricated in 5 mM electrolyte, is shown in Fig. 2B. The diffraction planes (210), (220), (221), (112), and (212) are indexed in a tetragonal-rutile phase of SnO_2. Also, the diffraction plane (004) is indexed in tetragonal phase of SnO. Thus, the average crystallite size was found to be 88.15 nm. The dislocation densities of samples S1 and S2 calculated by equation (3) [18].

$$\delta = \frac{1}{D^2} \qquad (3)$$

and found to be 6.9×10^{11} cm^{-2}, 1.28×10^{11} cm^{-2}, respectively. These values indicate that the sample S2 has better crystalline quality than sample S1. Furthermore, all the XRD peaks of this sample are sharp, which indicates high crystalline quality.
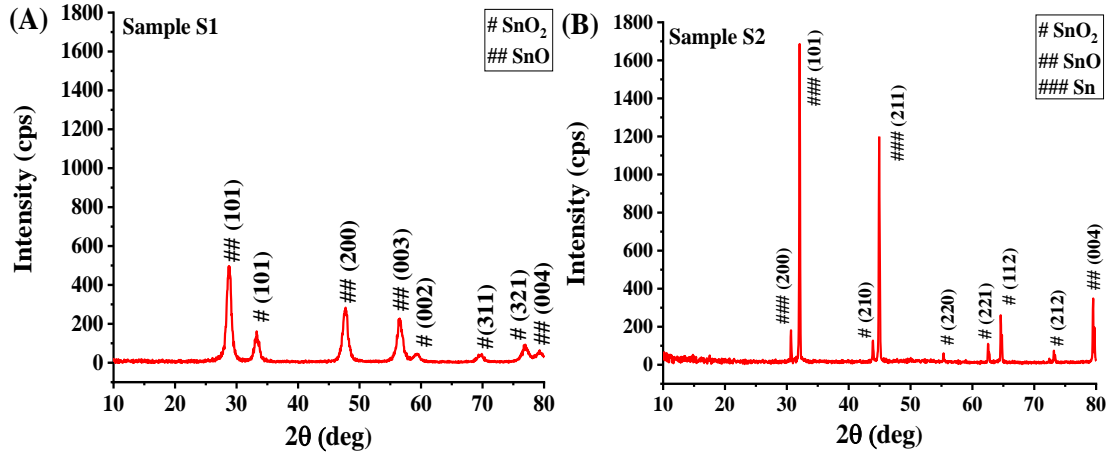
Fig. 2: The XRD pattern of SnO and SnO_2 Ns anodized at 5 V for 10 min using
(A)1 mM of electrolyte for sample S1 and (B) 5 mM of electrolyte for sample S2.

5.2 Morphological Properties

Figure 3 shows the FE-SEM images of tin oxide Ns. For sample S1, which was prepared by 1 mM electrolyte, formation of SnO_2 NPs with sizes between 47 and 61 nm over cracks regions can be seen in Fig (3A, B). For samples S2, whose electrolyte concentration was 5 mM, a spongy structure of nano-rocks with size of 71 - 89 nm is seen in Fig (3C, D). Thus, the structure morphology is highly changed when the concentration was changed. This behavior was previously studied and attributed to increase of oxygen evolution with more concentration [9].
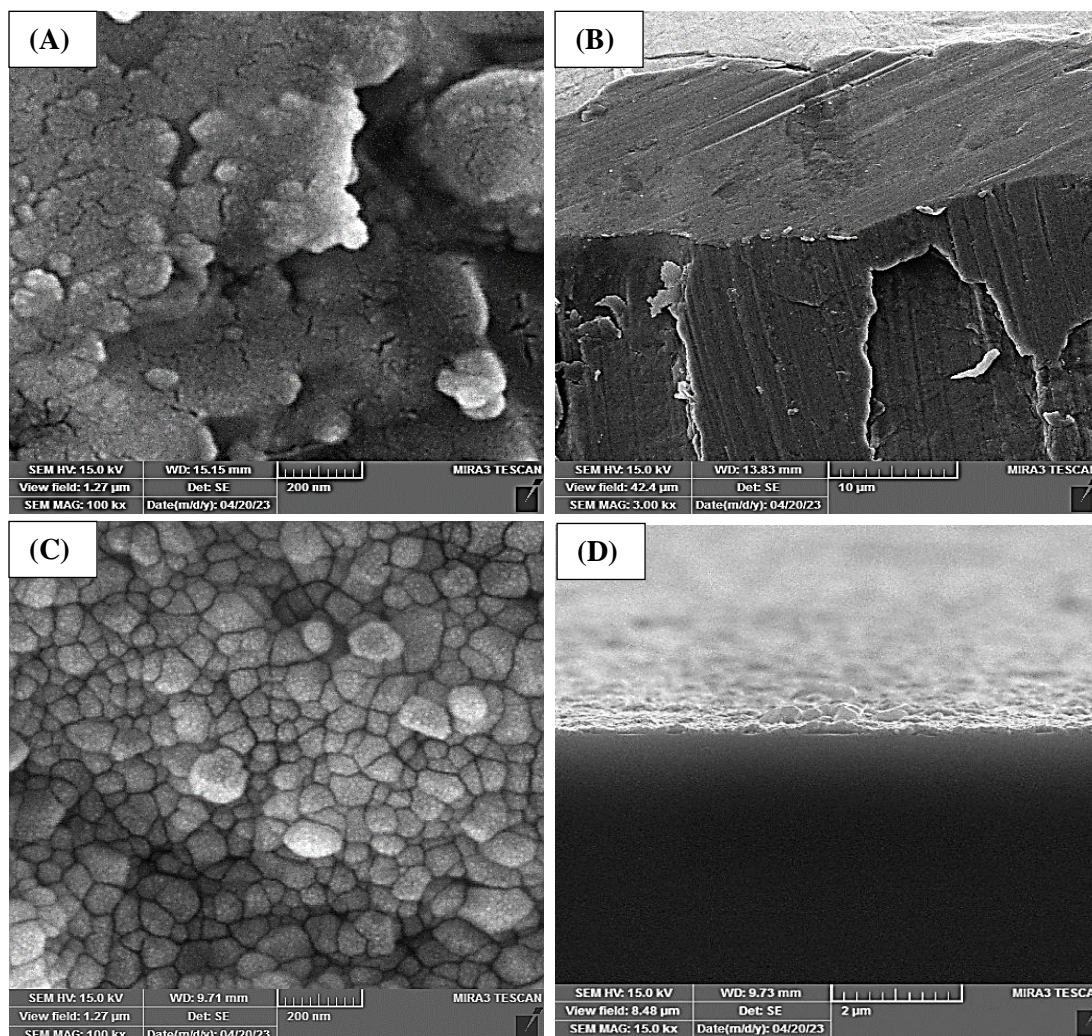
Fig. 3: The FE-SEM images of tin oxide Ns fabricated by electrochemical anodization in (A, B) 1 mM, and (C, D) 5 mM.

The EDX spectra, shown in Fig. 4, were performed to confirm the presence of the elements of the fabricated Ns. In sample S1, the peaks are related to the elements Sn (W% 84.41), oxygen (O) (W% 9.04), nitrogen (N), carbon (C), and iodine (I), as shown in Fig. (4 A). For sample S2, carbon defects are almost formed in the structure, decreasing the mount of the Sn element (W% 0.52), as shown in Fig. (4 B). According to the EDX spectra, the prepared nanostructures were confirmed to contain mainly Sn and O elements with small amounts of impurities, which could be added out of environment [19].
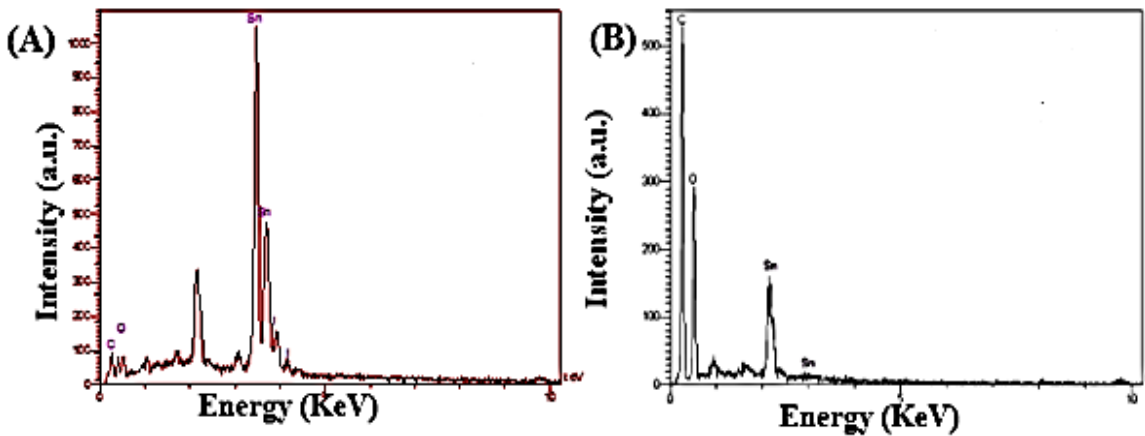
Fig. 4: The EDX spectra of SnO and SnO_2 Ns fabricated by anodizing a Sn foil.
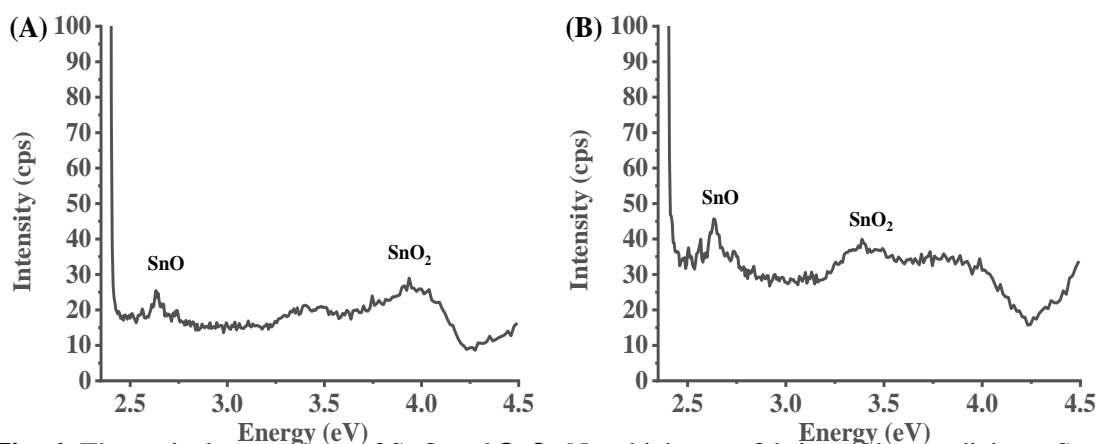(A) sample S1 and (B) sample S2.

Furthermore, the element mapping images of these samples, shown in Fig. 5, confirm the abundance of Sn and O elements.
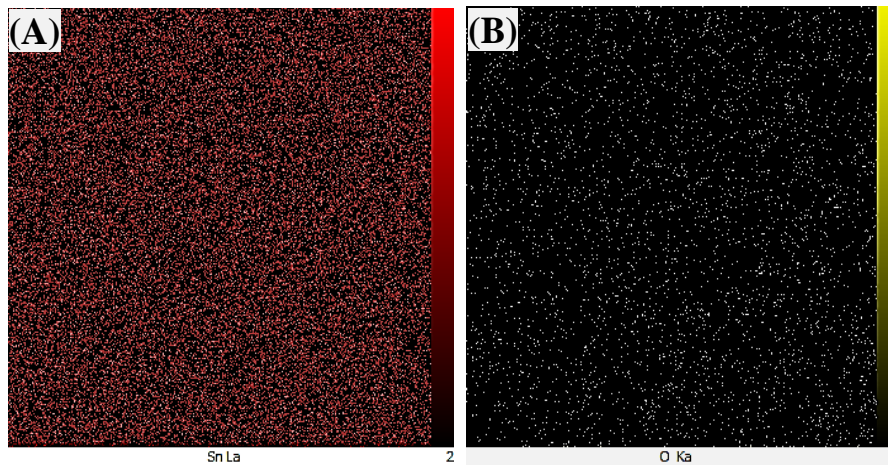
Fig. 5: The element mapping of SnO and SnO_2 Ns fabricated by anodization of Sn foil. (A) Sn element. (B) O element.

5.3 Optical Properties

Fluorescence spectra were achieved to estimate the energy gaps of the nanostructures using RF-5301 PC Shimadzu fluorophotometer. By stimulating the samples with light of a wavelength of 280 nm, the transition energy was determined at room temperature., and then, the energy gaps were estimated from the fluorescent spectra. In both samples, there exist SnO peaks at 2.64 eV, which consistent with the reported results [20]. For SnO_2 Ns, the peak seen at 3.93 eV refers to the blue-shifted energy gap when the particles size reduces due to quantum confinement effect. This finding is similar to the solvothermal synthesized SnO_2 Ns [21]. With increasing the concentration to 5 mM, the SnO_2 NS peak is seen in 3.37 eV, as shown in Fig. (6 B), which closes to the literatures of Ref [22, 23].

Fig. 6: The optical energy gap of SnO and SnO_2 Ns which were fabricated by anodizing a Sn foil. (A) sample S1 which was fabricated in 1 mM. (B) sample S2 which was fabricated in 5 mM.

5.4. Photoactivity Measurements

Figure 7 illustrates the photodegradation spectra of SnO_2 Ns, under sun irradiation of the MB dye for 140 min with intervals of 20 min. All the measurements were made by direct sunlight irradiation. For samples S1, the efficiency was calculated to be 85.83 % after 140 min of sunlight exposure, as shown in Fig. (7 A). The photodegradation of sample S2, shown in Fig. (7 B), the degradation efficiency was calculated to be 94.84 %. Thus, much enhancement in the efficiency by increasing the electrolyte concentration to 5 mM
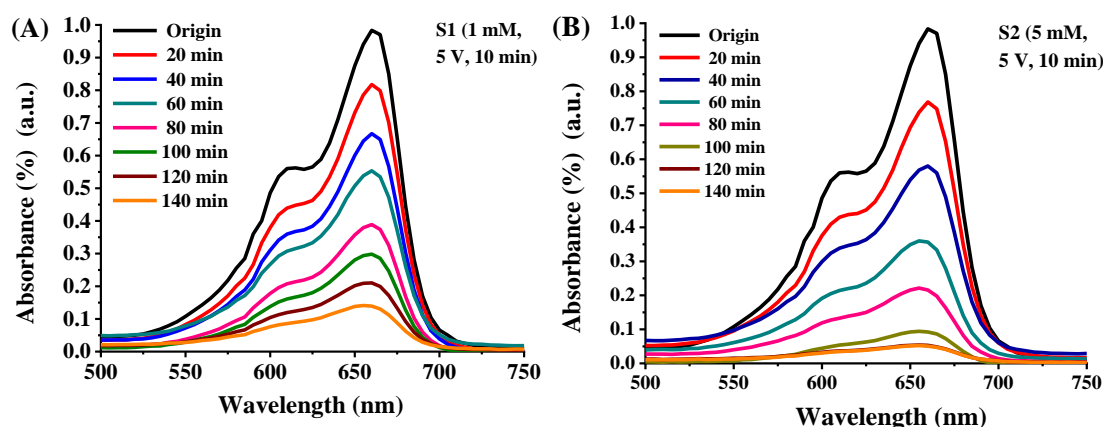

Fig. 7: The MB dye photodegradation spectra by the SnO_2 Ns which were fabricated by anodizing a Sn foil. (A) sample S1 which was fabricated in 1 mM. (B) sample S2 which was fabricated in 5 mM. The first-order rate kinetic constant (k) for the MB dye degradation for time (t), shown in Fig. 8, was evaluated by equation (4) [24]:

$$ln(\frac{C}{C_\circ}) = -kt \qquad (4)$$

The value of k was calculated to be 0.0138 min^{-1} for sample S1 and 0.0240 min^{-1} for sample S2, which are large compared with similar previous studies [25]. In general, sample S2 particularly improves the MB dye ability to degrade.
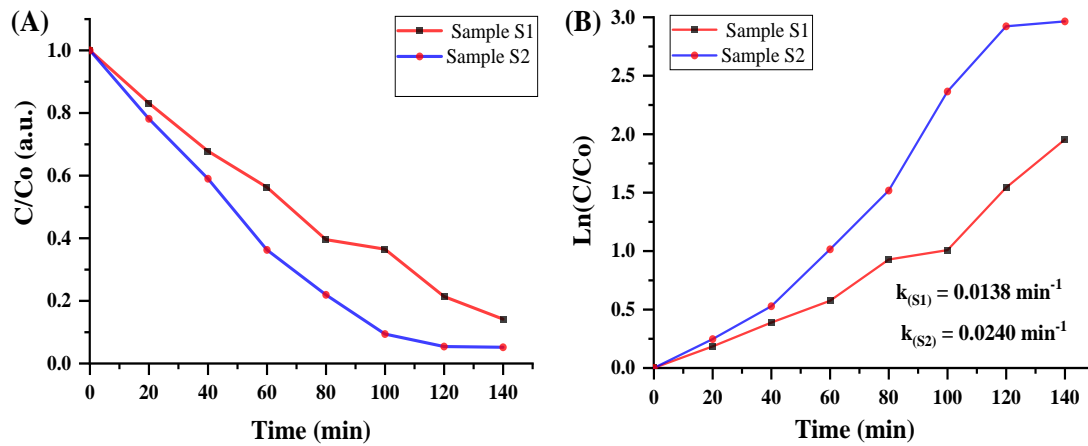
Fig. 8: (A) Kinetic degradation of the MB dye by SnO_2 Ns. (B) The first-order linear degradation rate of dye with time.

The high efficiency exhibited by sample S2 is a result of improving adsorption sites with more electron-hole separations [26]. Also, because of the low defect density, electron-hole recombination is decreased, with increasing the surface area, photoactivity was enhanced [27]. Thus, SnO_2 Ns are considered efficient photocatalysts for the degradation of MB dye when compared with a number of published researches, as listed in Table 1.

Table 1. Comparison of the photocatalytic efficiency of the submitted work with previous works.

Technique	Materials	Degradation Time (min)	Photocatalytic Efficiency (%)	Ref.
Hydrothermal	SnO_2 nanospheres	210	40.64	[28]
Green Synthesis	Pristine mono metallic SnO_2 NPs	195	35.7	[29]
Pulse laser Ablation-Hydrothermal	Spherical-like SnO_2 Ns	150	21.5	[15]
Modified Precipitation	SnO_2 NPs	180	79	[30]
Electrochemical Anodization	SnO_2 NPs	240	76.85	[19]
Electrochemical Anodization	SnO_2 Ns	140	94.84	Submitted Work

6. Conclusions

Unlike traditional preparation of SnO_2 porous, an electrochemical anodization technique was used to fabricate SnO_2 NPs. The electrolyte concentration was slightly changed to synthesis the nanoparticles, and thence, to enhance the photoactivity of the prepared NS. SnO and SnO_2 nanorocks and nanoparticles with a tetragonal crystalline phase were obtained. The energy gap was found to expand up to 3.93 eV depending on the concentration. Hence, with increasing the electrolyte concentration from 1 mM to 5mM, the photodegradation efficiency was highly enhanced, which reaches 94 % after two hours of sunlight exposure. It is inferred the dependence of morphology as well as the photoactivity on the anodization electrolyte concentration.

References

[1] Wang, H., Sun, F., Zhang, Y., Li, L., Chen, H., Wu, Q., & Yu, J. C. (2010). Photochemical growth of nanoporous SnO_2 at the air–water interface and its high photocatalytic activity. Journal of Materials Chemistry, 20(27), 5641.

[2] Wang, H., & Rogach, A. L. (2013). Hierarchical SnO_2 Nanostructures: Recent Advances in Design, Synthesis, and Applications. Chemistry of Materials, 26(1), 123–133.

[3] Das, S., & Jayaraman, V. (2014). SnO_2: A comprehensive review on structures and gas sensors. Progress in Materials Science, 66, 112–255.

[4] Chikunova, I. O., Semeykina, V. S., Kuznetsov, A. N., Kalinkin, P. N., Gribov, E. N., & Parkhomchuk, E. V. (2019). Template-assisted synthesis and electrochemical properties of SnO2 as a cathode catalyst support for PEMFC. Ionics. doi:10.1007/s11581-019-03327-4

[5] Yang, A., Tao, X., Pang, G. K. H., and Siu, K. G. G. (2007). Preparation of Porous Tin Oxide Nanobelts Using the Electrospinning Technique. Journal of the American Ceramic Society, 91(1), 257–262.

[6] Wasly, H.S., Abd El-Sadek, M.S., Elnobi, S. *et al.* (2022). Morphological, structural, and optical properties of flexible Tin Oxide(II) thin film via thermal evaporation technique. *Eur. Phys. J. Plus* **137**, 164.

[7] Bian, H., Tian, Y., Lee, C., Yuen, M.-F., Zhang, W., & Li, Y. Y. (2016). Mesoporous SnO2 Nanostructures of Ultrahigh Surface Areas by Novel Anodization. ACS Applied Materials & Interfaces, 8(42), 28862–28871.

[8] Zaraska, L., Bobruk, M., Jaskuła, M., and Sulka, G. D. (2015). Growth and complex characterization of nanoporous oxide layers on metallic tin during one-step anodic oxidation in oxalic acid at room temperature. Applied Surface Science, 351, 1034–1042.

[9] Zaraska, L., Gawlak, K., Gurgul, M., Gilek, D., Kozieł, M., Socha, R. P., and Sulka, G. D. (2019). Morphology of nanoporous anodic films formed on tin during anodic oxidation in less commonly used acidic and alkaline electrolytes. Surface and Coatings Technology, 362, 191 - 199.

[10]   Gao, Z., Cao, J., Muzammal, H. M., Wang, C., Sun, H., Chong, D., Wang, Y. (2019). Ultrasound assisted large scale fabrication of superhydrophilic anodized SnO_x films with highly uniformed nanoporous arrays. Materials Chemistry and Physics, 122540.

[11]   Li, P., Niu, D., He, M., Huang, H., Ying, Z., Xu, H., … Zhu, X. (2020). The Growth Model of Tin Anodizing Process and the Capacitive Performance of Porous Tin Oxides. The Journal of Physical Chemistry C. 124, 5, 3050–3058.

[12]   do Nascimento, J L, Iêda Maria G S, André Luiz M O, & Mary Cristina F A. (2022). The Influence of Synthesis Methods and Experimental Conditions on the Photocatalytic Properties of SnO_2 : A Review" Catalysts 12, no. 4: 428.

[13]   Kumar, V., Govind, A., & Nagarajan, R. (2011). Optical and Photocatalytic Properties of Heavily F–-Doped SnO_2 Nanocrystals by a Novel Single-Source Precursor Approach. Inorganic Chemistry, 50(12), 5637–5645.

[14]   Kajbafvala, A., Ghorbani, H., Paravar, A., Samberg, J. P., Kajbafvala, E., & Sadrnezhaad, S. K. (2012). Effects of morphology on photocatalytic performance of Zinc oxide nanostructures synthesized by rapid microwave irradiation methods. Superlattices and Microstructures, 51(4), 512–522.

[15]   Abbas, Khaldoon N.; Hussain, Nedal A.; Nusseif, Asmaa D.; Hussein, Emad H.; Aziz, Wisam J.; Salim, Ali A. (2020). Fabrication and photocatalytic characterization of SnO_2 and SnO_2 / TiO_2 nanostructure films. Journal of Physics: Conference Series, 1484, 012002.

[16]   Suthakaran, S., Dhanapandian, S., Krishnakumar, N., & Ponpandian, N. (2019). Hydrothermal synthesis of SnO_2 nanoparticles and its photocatalytic degradation of methyl violet and electrochemical performance. Materials Research Express, 6(8), 0850i3.

[17]   Iqbal, M. Zubair & Wang, Fengping, Hussain, Riaz, and et al., (2014). Time-Dependent Growth and Optical Properties of Stannous Oxide Architectures. Materials Focus.3 (2), 92-97.

[18]   Sharmin, M ., Rahaman, M ., Hussain, K ., Das, C, & Choudhury, S. (2016). Structure, Morphology and Opto-Electrical Properties of Nanostructured Indium Doped SnO_2 Thin Films Deposited by Thermal Evaporation. European Scientific Journal,12 (27) 1857 – 7881.

[19]   Wang, J, Lu, C, Liu, X, Wang, Y, Zhu, Z, and Meng, D, (2017). Synthesis of tin oxide (SnO & SnO_2) micro/nanostructures with novel distribution characteristic and superior photocatalytic performance. Mater. Des, 115, 103–111.

[20]   Manouchehri, S, Boroojerdian, P, Marasi, A, Amoo, and M, Yousefi, M H, (2018). Synthesis of Single Phase Tin(II) Oxide Nanoparticles by Microwave-Assisted Hydrothermal Technique. Iran. J. Chem. Chem. Eng. 37 (6).

[21]   Anadan, K. and Rajendran, V. (2010). Solvents effect of quantum sized SnO_2 nanoparticles via solvothermal process and optical properties. Mat. Sci. Res. India, 7(2), 389-397.

[22]   Siva Kumar, V. V., & Kanjilal, D. (2017). Structural, optical and transport studies of nanocomposite SnO x thin films grown by DC sputter deposition and post-annealing. Materials Research Express, 4(2), 026403.

[23]   Kumar, V., Som, S., Neethling, J. H., Olivier, E., Ntwaeaborwa, O. M., & Swart, H. C. (2014). The role of surface and deep-level defects on the emission of tin oxide quantum dots. Nanotechnology, 25(13), 135701.

[24]   Jiang, H., Wang, R., Wang, D., Hong, X., & Yang, S. (2019). SnO_2/Diatomite Composite Prepared by Solvothermal Reaction for Low-Cost Photocatalysts. Catalysts, 9(12), 1060.

[25]   Kar, A, Olszówka, J, Sain, S, and ea al., (2019). Morphological effects on the photocatalytic properties of SnO_2 nanostructures. J. Alloys Compd. 810 151718.

[26]   Ma, C M, Hong, G B, and Wang, Y K (2020). Performance Evaluation and Optimization of Dyes Removal using Rice Bran-Based Magnetic Composite Adsorbent. Materials, 13(12), 2764.

[27]   He, Z., Zhu, Z., Li, J., Zhou, J., and Wei, N. (2011). Characterization and activity of mesoporous titanium dioxide beads with high surface areas and controllable pore sizes. Journal of Hazardous Materials, 190 (1-3), 133–139.

[28]   Sephra, P. J., Baraneedharan, P., Sivakumar, M., Thangadurai, T. D., and Nehru, K. (2018). Size controlled synthesis of SnO_2 and its electrostatic selfassembly over reduced graphene oxide for photocatalyst and supercapacitor application. Materials Research Bulletin, 106, 103–112.

[29]   Liaqat, F., Vosqa, U. T., Khan, F., Haleem, A., Shaik, M. R., Siddiqui, M. R. H., and Khan, M. (2023). Light-driven catalytic activity of green-synthesized SnO_2/WO_3−X hetero-nanostructures. ACS Omega. 24, 8(22), 20042-20055.

[30]   Kim, S. P., Choi, M. Y., and Choi, H. C. (2016). Photocatalytic activity of SnO_2 nanoparticles in methylene blue degradation. Materials Research Bulletin, 74, 85–89.